



Observations of an inshore front associated with the Chesapeake Bay outflow plume

G.O. Marmorino*, T.F. Donato, M.A. Sletten, C.L. Trump

Remote Sensing Division, Naval Research Laboratory, Code 7250, Washington, DC, 20375-5351, USA

Received 22 January 1999; received in revised form 6 August 1999; accepted 23 September 1999

Abstract

Preliminary observations are reported of a recurring front located near Cape Henry, Virginia, USA. The front occurs on the right-hand side, looking seaward, of the buoyant plume discharging from the Chesapeake Bay and separates the plume from a band of relatively dense seawater confined against the Virginia coast. The front thus appears to be of a type similar to the inshore plume front reported by Sanders and Garvine for the Delaware Bay. Similar to an estuarine tidal intrusion front, the Cape Henry front evolves to a prominent V-shaped planform during flood tide and subduction of fluid along the front may provide a means for recirculation of near-surface material. © 2000 Elsevier Science Ltd. All rights reserved.

Keywords: Ocean front; Buoyant discharge; Estuary–ocean interaction; Chesapeake Bay

1. Introduction

The discharge of buoyant water from large estuaries, such as the Chesapeake Bay, tends to bulge outward over the continental shelf before forming a downstream current (coastal jet) trapped by the Earth's rotation along the right-hand coast (e.g., Boicourt et al., 1987; Wiseman and Garvine, 1995; Chao, 1988). Tidal modulation near the estuary mouth typically produces along the seaward edge of the discharge a strong salinity front, which delineates the buoyant outflow from well-mixed, dense shelf water and which moves outward with the ebbing tidal current. Such fronts are characterized by strong convergence of surface flow and downwelling (e.g., O'Donnell et al., 1998). Surface waves are steepened and break as they interact with converging

* Corresponding author. Tel.: + 1-202-767-3756; fax: + 1-202-767-3303.

E-mail address: marmorino@nrl.navy.mil (G.O. Marmorino)

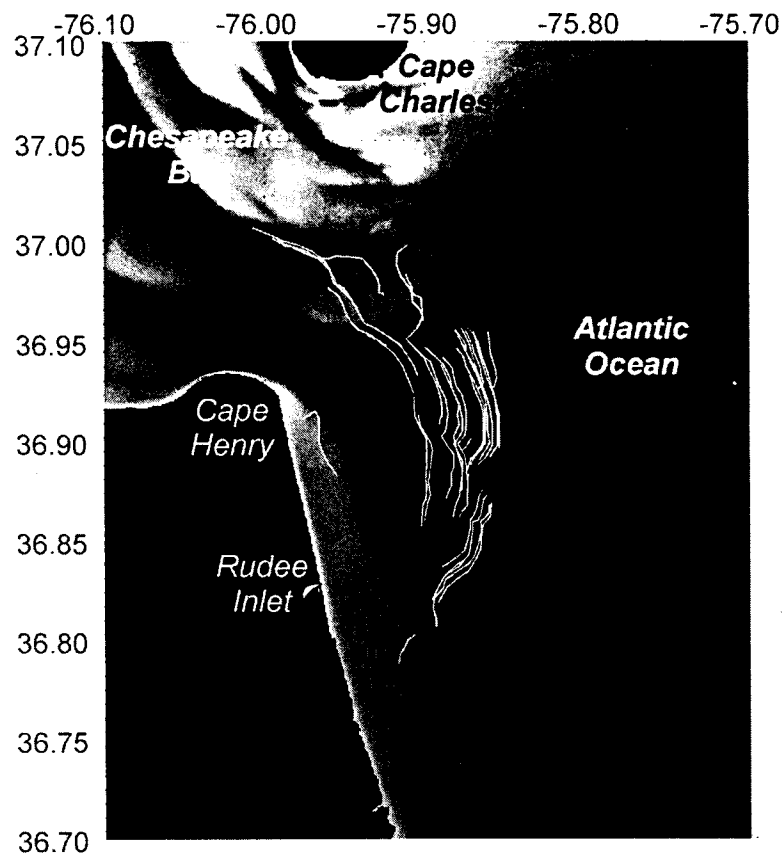


Fig. 1. Study area. Bathymetry is indicated by a linear gray-scale (white: sea level; black: depth and land). Curves show plume-edge frontal segments observed with airborne real-aperture radar in 1997, during the second Chesapeake Bay Outflow Experiment (COPE-2). The large grouping of curves to the east shows successive positions of the offshore front as observed during ebb tidal flow on May 9. A single curve near Cape Henry shows the inshore front observed during flood tide on May 9.

surface frontal currents, so that the plume boundary can appear as a distinct signature in a radar image of the sea surface (e.g., Volgelzang et al., 1997). The evolution of an individual outflow pulse can thus be studied by mapping successive positions of the plume front using a time series of such images.

Such a mapping has recently been accomplished using airborne imaging radar (Marmorino et al., 1999). An example is shown in Fig. 1. The large grouping of curves located east of Cape Henry shows time-sequential positions of the front associated with the leading-edge of the most-recently ebbing bay water. The radar signature of the plume extends approximately continuously from inside the bay, where it tends to follow the north wall of the Chesapeake Channel, to a seaward-extending bulge located about 20 km east of Cape Henry and this translates across the shelf at a mean speed of about 36 cm/s. The signatures tend to curve inward toward the Virginia shoreline indicating the transition to the coastal jet occurs south of Rudee Inlet. During late flood tidal flow, however, an additional radar signature appears inshore of about 10 kilometers off the Virginia coastline near Cape Henry. A single example of this signature is shown in Fig. 1. It consists of a northern segment oriented approximately across-shore and an adjoining segment extending southward, approximately

shore. We will show that these two segments delineate the frontal boundary of a plume of dense water confined alongshore by the buoyant outflow of the plume. The inshore front thus forms an inner or inshore edge to the plume, which is in contrast to the outer or offshore edge that propagates seaward over time. An apparently similar pattern of fronts has been observed near the mouth of Delaware Bay (Sanders and Garvine 1996). The inshore front is thus of general interest, and it may play some role in the recirculation of material near the mouth of a bay.

2. Experiment background and instrumentation

2.1. The Chesapeake Bay Outflow Plume Experiment (COPE)

Measurements were made during two Chesapeake Bay Outflow Plume Experiments conducted in September 1996 (COPE-1), and May 1997 (COPE-2). These programs involved a number of investigators and measurement techniques (Marmorino et al. 1998; Sletten et al., 1999). Data analyzed in this paper were collected aboard an aircraft flying an imaging radar and aboard a research ship. A major objective was to acquire simultaneous in situ and remote sensing data having sufficient resolution to allow study of the development and subsequent evolution of the outflow plume in the near-field region, i.e., the region of the bulge extending seaward from the bay mouth. The two experimental periods were chosen to compare conditions of low autumn discharge with high vernal discharge. However, tropical storms produced a September streamflow into the bay of about 4000 m³/s (well above normal), while the discharge during the May 1997 sampling period was about 2300 m³/s, which is in the range of normal springtime values. (See Sletten et al. (1999) for details.) Thus, the measurements reported in this paper were made under conditions of high to moderate outflow, varying by nearly a factor-of-two between the two periods.

A number of comparisons will be made with predicted tidal current. These were obtained from a tidal station at 36.93°N, 75.99°W, which is located about 2 km north-northeast of Cape Henry.

2.2. Airborne radar measurements

An airborne X-band radar system, deployed on an NRL P-3 Orion aircraft, was used to either map the entire study area (at roughly hourly intervals) or repeatedly image a specific feature of interest. The resulting images have a range resolution of about 10 m and an azimuthal (along-track) resolution of about 25 m at a range of 2 km. The time to acquire a typical image was 1–2 min, and the mid-image incidence angle is 60°. Image location is obtained using precision-coded Global Positioning System (GPS) data; however, uncertainty in the timing between the radar and the datstreams resulted in an along-track position uncertainty of the order of 100 m. The relatively high spatial resolution of the data and the ability to make time-sequential measurements made it possible to delineate features resulting from a particular cycle in progress and to study plume interactions with varying bathymetry.

water masses on the continental shelf (Sletten et al., 1999). The radar measurement used horizontal polarization and low illumination angles to increase sensitivity to the small-scale structures associated with wave breaking. A front thus appears in imagery as a narrow region of high signal levels relative to the background. The airborne radar measurements made during COPE-2 sampled the inshore front, and only these are shown in this paper.

2.3. Shipboard measurements

In situ measurements were made aboard the R/V *Cape Henlopen*. Currents in the inshore front were measured during COPE-1 using a 600 kHz broadband acoustic Doppler current profiler (ADCP) towed to the side of the ship to avoid surface water disturbed by the ship's wake (e.g., Marmorino and Trump, 1996). The ADCP measurement is centered at 2.2 m depth and the depth resolution is 0.5 m. Mounted just below the ADCP were an optical transmissometer (0.6 m depth) and a conductivity-temperature sensor (0.7 m depth). More extensive in situ data and ADCP data are available from COPE-1. Additional current measurements were made in COPE-2 using a horizontally scanning ADCP. This was a 3 narrowband unit deployed at 0.6 m depth from a support pole mounted on the side of the ship (Marmorino et al., 1999a). Also, during COPE-1, a navigation radar system was deployed aboard the ship and used to record an image of the surface at 1 min intervals (Marmorino et al., 1999b). A frontal orientation and frontal planform could be extracted by carefully examining a number of consecutive images, but the signal contrast was very low and so we do not show any shipboard images in this paper.

3. Results

Results from the September 1996 and May 1997 campaigns are presented in this section. We begin (Section 3.1) with an overview of the airborne radar imagery.

Table 1

Summary of frontal observations made in September 1996, and May 1997

Date	Tidal phase	Frontal motion ^a	Wind		Salinity	
			Dir	Speed (m/s)	Coastal band	P
9/20	Flood	No data	NW	5	≈ 23	<
9/23	Ebb to flood	No data	W	12	≈ 23	<
9/25	Late flood to Ebb	S	W	6	28	≈
5/5	Early flood	N	SE	< 5	No data	N
5/9	Flood	S	SW	< 5	28	≈
5/16	Ebb to flood	N	W	6	≈ 24	≈
5/22	Late flood	No data	NW	8	≈ 25	≈

^a Frontal motion is the direction toward which the across-shore frontal segment moved.

obtained in May 1997; Sections 3.2 and 3.3 present two frontal evolution studies using the May imagery and examples of nearly simultaneous in situ data; Section 3.4 presents two additional cases of in situ data from September 1996, which complement and extend the results from the May data. Conditions during these various cases are summarized in Table 1.

3.1. Overview of airborne radar imagery

Fig. 2 shows four airborne radar images of the coastal area between Cape Henry and Rudee Inlet, each collected on a different day and under different wind conditions (see Table 1). Each map-referenced image contains a different type of expression of the inshore front, though this can be partly obscured by ambient scattering and air-sea roll-induced variability. Images acquired during flood tide (e.g., Figs. 2(a) and 2(b)) typically show the front extending to very near Cape Henry. Details of the frontal structure do vary, however. For example, in Fig. 2(a) the front has a single sharp cusp at its most northern extent, while in Fig. 2(b) the front has several less pronounced cusps. In Fig. 2(c), which corresponds to 1.1 h before predicted flood, the frontal signature has the appearance of an inverted 'U', suggesting a northward-intruding water mass centered about 1.5 km from shore; subsequent imagery (not shown) reveals a frontal signature nearer Cape Henry and extending more across-shore (Figs. 2(a) and (b)). Fig. 2(d), which was acquired during northwesterly winds and flood tide, shows an alongshore frontal segment located 1.5 km offshore and about 10 kilometers north of Rudee Inlet.

3.2. Frontal evolution study: 9 May 1997

Time sequences of images available on particular days have been examined to reveal details of frontal evolution. Fig. 3 shows a sequence of four images collected on 9 May 1997, spanning the period from 0.5 to 3.4 h into flood tide. Early in flood (Figs. 3(a) and 3(b)) the front is already well developed and shows a number of cusps, each separated by about 700 m. (A mapped version of the Fig. 3(b) image is shown in Fig. 2(b).) About 2 hours later (Fig. 3(c)), across- and alongshore frontal segments meet in a right-angle bend; additional small-scale features can be seen on the alongshore frontal segment. The final image (Fig. 3(d)), just after maximum flood, shows a distinct V-shaped frontal apex. Thus, there are some subtle changes over time in the frontal planform, including a tendency, as flood progresses, towards a distinct apex at the most northward frontal position.

Simultaneous with the radar measurements, data were being collected aboard the R/V *Cape Henlopen*. (The ship appears as a bright spot in each of the radar images in Fig. 3). A continuous record of salinity at 1 m depth (not shown) shows values alternating between 22 and 28.5 psu as the ship sailed back and forth across the front, the saltier water lying consistently southwest of the front. Thus the frontal signature shown in Fig. 3 bounds a mass of salty water against the coast and separates it from the less-dense plume water. All the along-front cusps as well as the frontal apex appear in the imagery thus point seaward into the plume water. Shipboard measurements

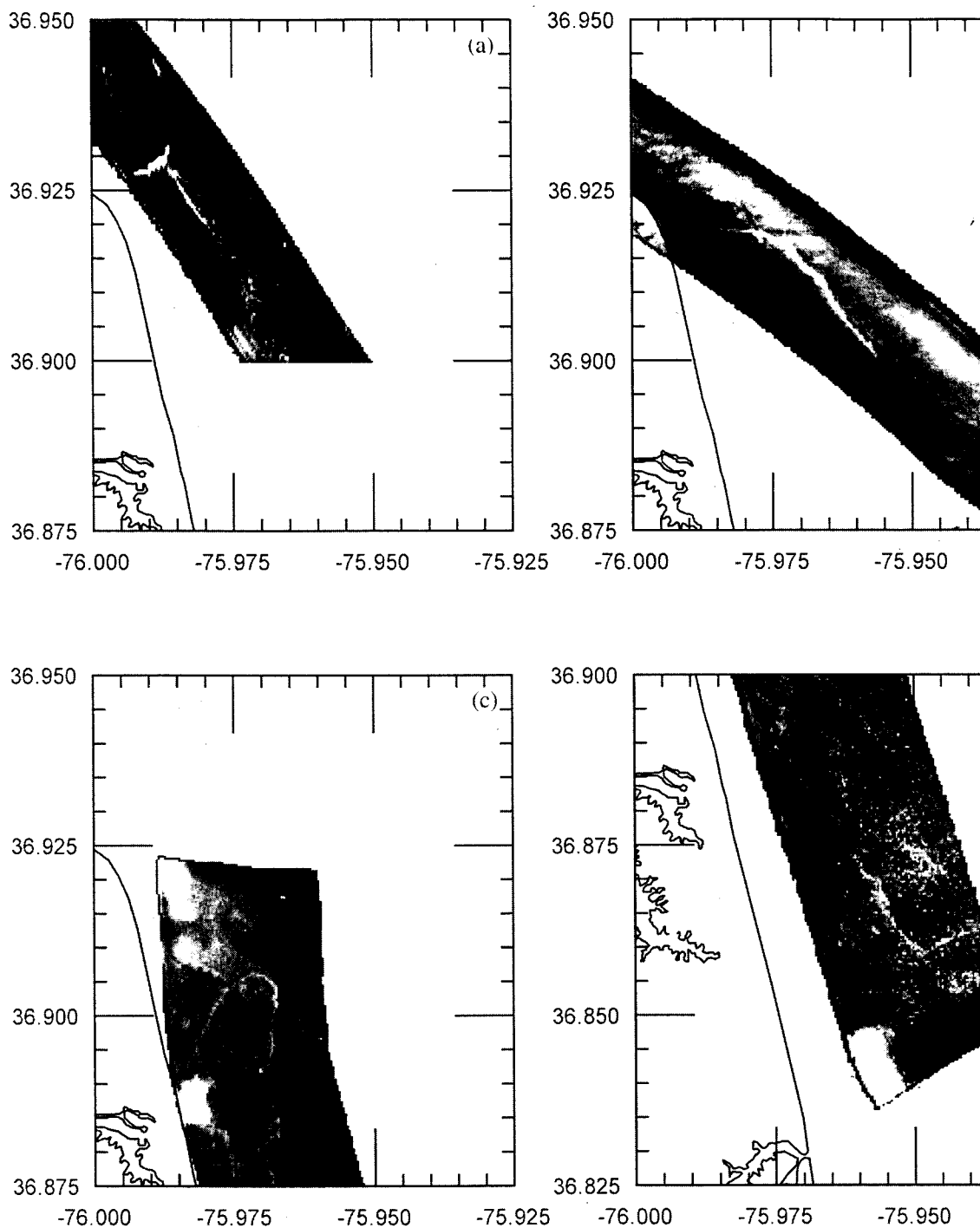


Fig. 2. Sample airborne radar images showing the inshore front under different wind conditions stage. (a) 5 May (Pass 10). (b) 9 May (Pass 14). (c) 16 May (Pass 22). (d) 22 May (Pass 1; wave signature lies roughly alongshore). The front appears as a nearly continuous bright (white) curve, indicating a narrow band of steepened and breaking waves; other areas of elevated signals correspond to scattering from the wind-roughened surface, and adjacent white and black areas result from air-sea interface. Images (a,b) correspond to 0.6 and 0.85 h into predicted flood tide; image (c) to 1.10 h before flood; image (d) to 4.0 h into flood.

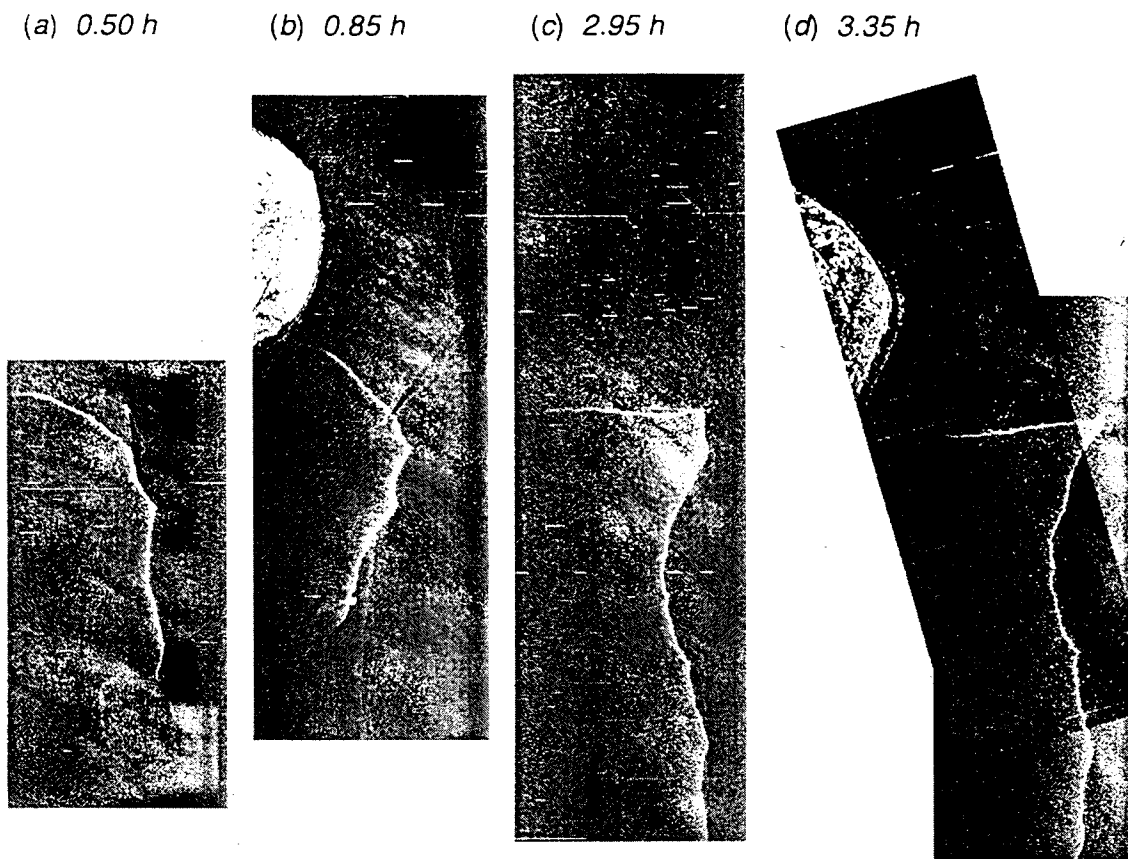
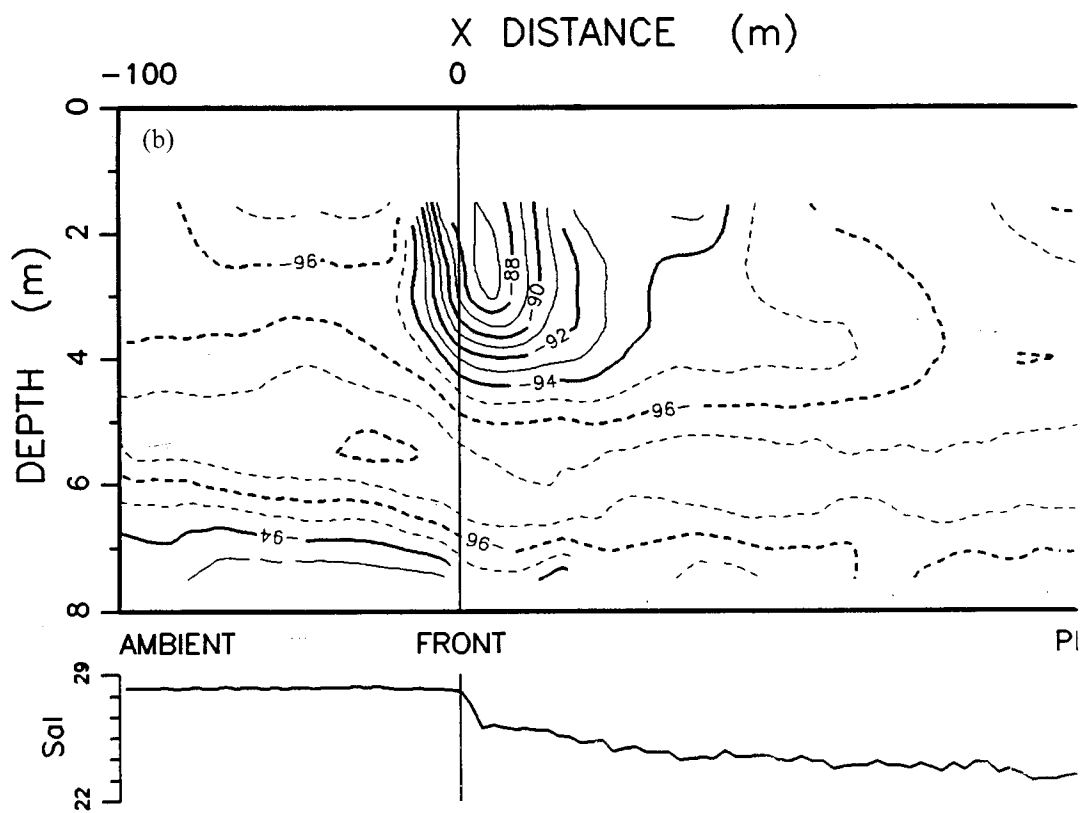
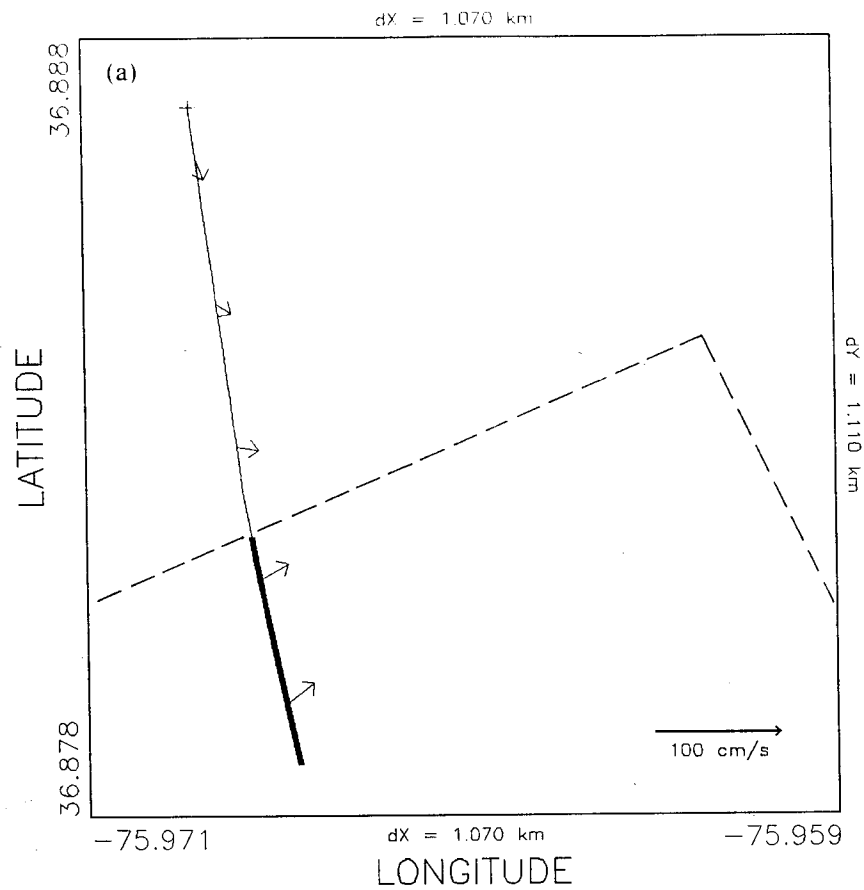


Fig. 3. Time sequence of airborne radar images showing evolution of the front near Cape Henry on 9 June 1997. (a) 0910 LT (Pass 8), 0.50 h into flood tide. (b) 0930 LT (Pass 14), 0.85 h into flood tide. (c) 1130 LT (Pass 44), 2.95 h into flood tide. (d) 1205 LT (Pass 52/54 composite), 3.35 h into flood tide. Each radar image has a width of about 2 km and a slightly different absolute orientation. A mapped version of the image in (a) appears in Fig. 2(b) and the digitized frontal signature from the image in (c) is shown in Fig. 1 as the closest to Cape Henry.

were not made inshore of the 7 m isobath; however, inferences about conditions in shallower water can be made by noting that the airborne imagery shows the frontal signature extending into shallow water. Visual observations made from the ship showed the front extending toward the beach. It is reasonable to assume therefore that the changes measured across the front in deeper water may be extrapolated to near shore.

Current measurements are unavailable for the Fig. 3 period, but Fig. 4(a) shows ADCP data that were collected 2 h after the image shown in Fig. 3(d). By this time, even though the tide was still in flood, the front had translated about 3 km southward. (The frontal crossing position is indicated in later Fig. 7 as data point '3'.) Fig. 4 shows that north of the front the near-surface current is about 20 cm/s and directed approximately toward the southeast. South of the front, the current is 30 cm/s toward the northeast and approximately parallel to the front, which is indicated by a dashed line in the figure. (The orientation of the front was determined from radar pass which was made 43 min before the ship crossed the front.) There is thus a convergence and shear across the front with the change in the front-normal velocity.



being about 10 cm/s. A striking feature of the ADCP data is the behavior of acoustic backscatter intensity. Fig. 4(b) shows a vertical section of intensity data a 300 m long subset across the front. Highest intensity values occur in a narrow zone very near the surface frontal position as based on the salinity change at 0.7 m depth (see salinity trace at bottom of Fig. 4(b)). Compared with ambient levels of about -96 dB (relative dB units are used), levels near the front increase to -87 dB. This increase can be assumed to result from air bubbles injected into the water as the result of wave breaking along the front (e.g., Thorpe, 1982; Marmorino and Trump, 1995). The abrupt drop in salinity (by about 2 psu) suggests a strong local mixing between the plume and ambient water and high values of intensity penetrating to a depth about 4.5 m suggests a localized sinking of the near-surface water. A more gradual decrease in salinity occurs over 200 m on the plume side of the front, suggesting a broad mixing zone between the plume and underlying ambient water.

3.3. Frontal evolution study: 16 May 1997

Fig. 5 shows a sequence of four radar images collected on 16 May 1997. These images span 1.5 h before to 1.4 h after the onset of flood tide. The images are approximately aligned horizontally in latitude, with Cape Henry being visible in Figs. 5(a) and 5(b). A mapped version of the image in Fig. 5(b) appears in Fig. 2(c). More than an hour before flood, Figs. 5(a) and (b) already show a clear frontal signature about 2 km south of Cape Henry. The front penetrates farther north over time, reaching a position north of Cape Henry in Fig. 5(d) at 1.4 h into flood. Fig. 5(d) is thus similar to the imagery of 9 May that was acquired at about the same point in the flood phase. Details of frontal shape vary between the images but a common feature is a sharp bend or seaward-protruding apex that intensifies during flood tide, and shipboard observations made subsequent to Fig. 5(d) show the development of a V-shape similar to that in Fig. 3(d).

Salinity measurements made across the front on 16 May showed 21 psu water in the plume and 24 psu water along the coast. This is a smaller salinity contrast than found on 9 May, the difference likely being related to differences in the wind history (Section 4.2). An example of ADCP measurements collected simultaneously with the radar data is shown in Fig. 6. In this case, the measurements were made using a 300

Fig. 4. Towed ADCP measurements made from 1402 to 1407 LT, about 2 h after the image shown in Fig. 3(d). The measurements were made using a downward-looking ADCP towed from the ship. (a) Vector plot showing 1 min averaged 2 m depth currents plotted along the track of the ship, which begins in the upper left ("+" sign), extends approximately 1 km southward, and crosses the front at 1405 LT. The thick (thin) portion of the ship's track indicates salinity values greater (less) than 27 psu. The orientation of the front (shown schematically by the dashed line segment) derives from airborne radar measurements made at 1320 LT (Pass 74). (b) Vertical section of acoustic backscatter intensity I (units of relative decibels) over a 300 m subset across the front. Values of $I \geq -94$ dB (solid contour lines) are associated with the downwelling and entrainment of air bubbles injected by surface waves breaking along the front. The data portrayed in this section have an effective horizontal resolution of about 10 m and a vertical resolution of 1 m. Bottom depth is about 8.5 m. Horizontal distance x is measured perpendicular to the front. Near-surface salinity (bottom of figure) shows 28.5 psu ambient water ($x < 0$ m) and relatively fresh plume water ($x > 0$ m).

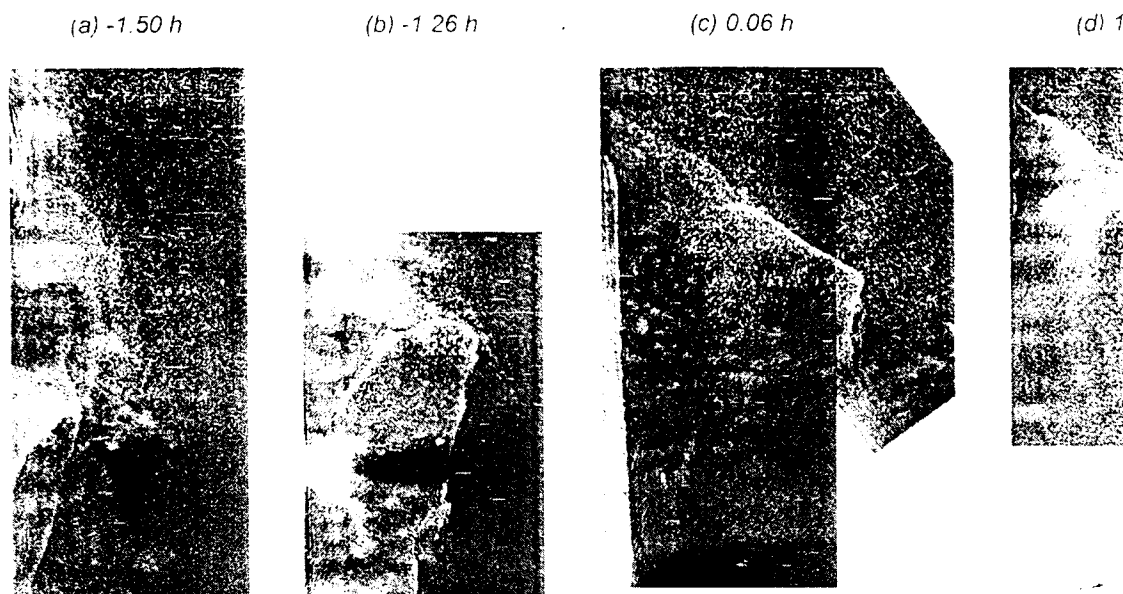


Fig. 5. As in Fig. 3 but for 16 May 1997. (a) 1330 LT (Pass 19), 1.5 h before onset of flood tide. (b) (Pass 22), 1.26 h before flood. (c) 1452 to 1504 LT (Pass 34/35 composite), 0.06 h into flood. (d) (Pass 049), 1.38 h into flood. The Virginia Beach coastline appears as a thin strip along the edge of each image; Cape Henry appears in the upper-left of (a). The images, which vary in orientation, show a northward progression of the front. Weak signals (most noticeable in panel d) derive from ship traffic located northeast of the imaged area. A mapped version of the image in (b) is in Fig. 2(c).

ADCP to scan horizontally from the ship (Section 2.3). The data in Fig. 6 are as time (x -axis) vs range from the instrument (y -axis). The ship's speed (1.4 m/s) and heading (180° T) were approximately constant over the period shown, and so the data are essentially horizontal maps of near-surface velocity and acoustic backscatter acquired over about a 2.3 km southward distance (27 min period). The horizontal planform of the front is clearly delineated in the intensity map as a narrow band of high values. (Intermittency in the signal is caused by rolling motion of the ship.) The band shows four prominent waveforms resembling the frontal cusps seen in the radar imagery. These cusps point toward the plume water and are separated by trough-like regions. The northernmost cusp (left side of figure) is the most prominent and corresponds to the frontal apex appearing in the radar imagery (Fig. 5). The frontal shape can be discerned in the velocity measurements. In the velocity plot, changes in the range direction (velocity gradient) are meaningful. In the initial part of data (left side of plot) there is no frontal signature in the intensity plot and no velocity gradient appears. Once the frontal signature appears, a maximum velocity change across the front of about 50 cm/s can be discerned. The width of the region over which the velocity changes is comparable with the width of the intensity signature, about 10 m. Thus the frontal convergence rate can be estimated as being of the order of 0.05/s (0.5 m/s over 10 m). This high value is responsible for the strong radar return and is comparable to the high values measured by O'Donnell et al. (1998) at the Connecticut River plume and by Marmorino and Trump (1996) in the James River. Both the backscatter and velocity contrasts weaken toward the south (right-hand side of figure).

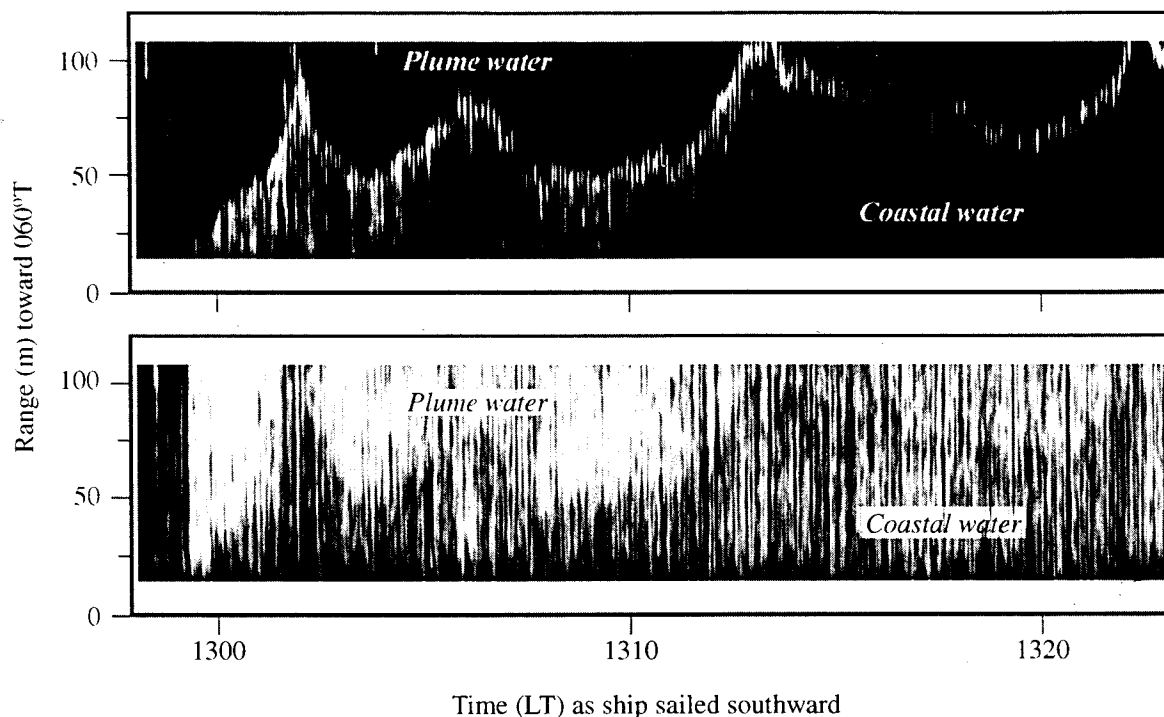


Fig. 6. Time-range maps derived from “horizontal” ADCP measurements made from 1258 to 1325 May 1997, just prior to the image shown in Fig. 5(b). (Top) Acoustic backscatter intensity, white signal being 10 dB higher than black; (bottom) relative velocity along a direction approximately normal to the front, black-to-white contrast being 50 cm/s. The x-axis corresponds to approximately 2.3 km south distance and the y-axis shows range from the instrument toward 60°T; thus the plume water lies toward the top of each panel. A continuous band of relatively high values of backscatter intensity delineates the horizontal planform of the front, which shows many of the same features as in the radar imagery; identical frontal shape can be discerned in the velocity contrast. Both the backscatter signal and velocity contrasts are weaker in the right-hand portion of the figure, which corresponds to the southern end of the inshore front.

of figure), which is similar to the trend of weakening contrast apparent in the radar imagery.

3.4. *In situ* data from September 1996

In this section we examine additional *in situ* data that were collected on different days during COPE-1. The first case (25 September 1996) focuses on an across-shore frontal segment such as shown in Figs. 2(a) and (b). The second example (23 September) focuses on an alongshore frontal segment such as in Fig. 2(d).

Sampling on 25 September was begun 2 km southeast of Cape Henry and extended from late flood to the beginning of ebb. Winds were westerly at about 6 m/s. The ship made 15 consecutive crossings of the across-shore frontal segment, which was oriented approximately normal to the coastline. As flood weakened, the front moved southward at an accelerating rate. Frontal positions for crossings 4 and 14 are shown in Fig. 7 (data points 1 and 2). For comparison the frontal position for the 9 May (Fig. 4) is also shown (data point 3). Relative to onset of flood tide, crossing 14

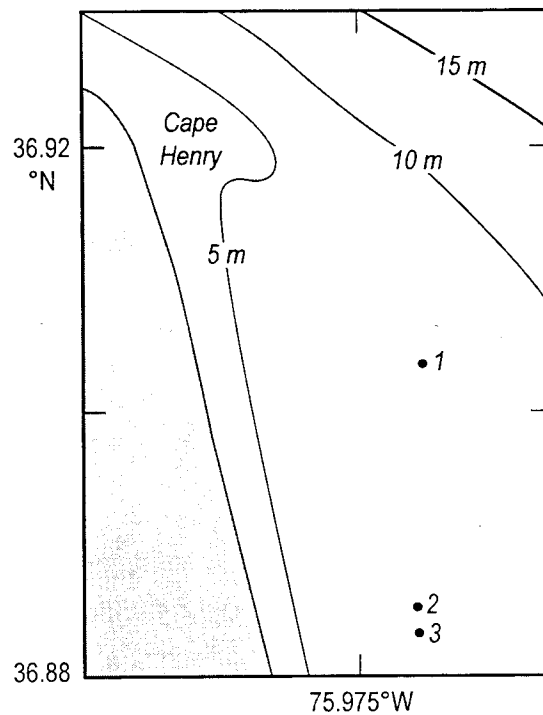


Fig. 7. Locations of frontal crossings 4 and 14 (1, 2) made on 25 September 1996 compared with crossing (3) made on 9 May 1997. Relative to the onset of flood tide, the frontal crossings occurred at +4.1 h, +5.5 h, and +5.4 h, respectively. ADCP data corresponding to the three crossings are shown in the subsequent two figures and in Fig. 4.

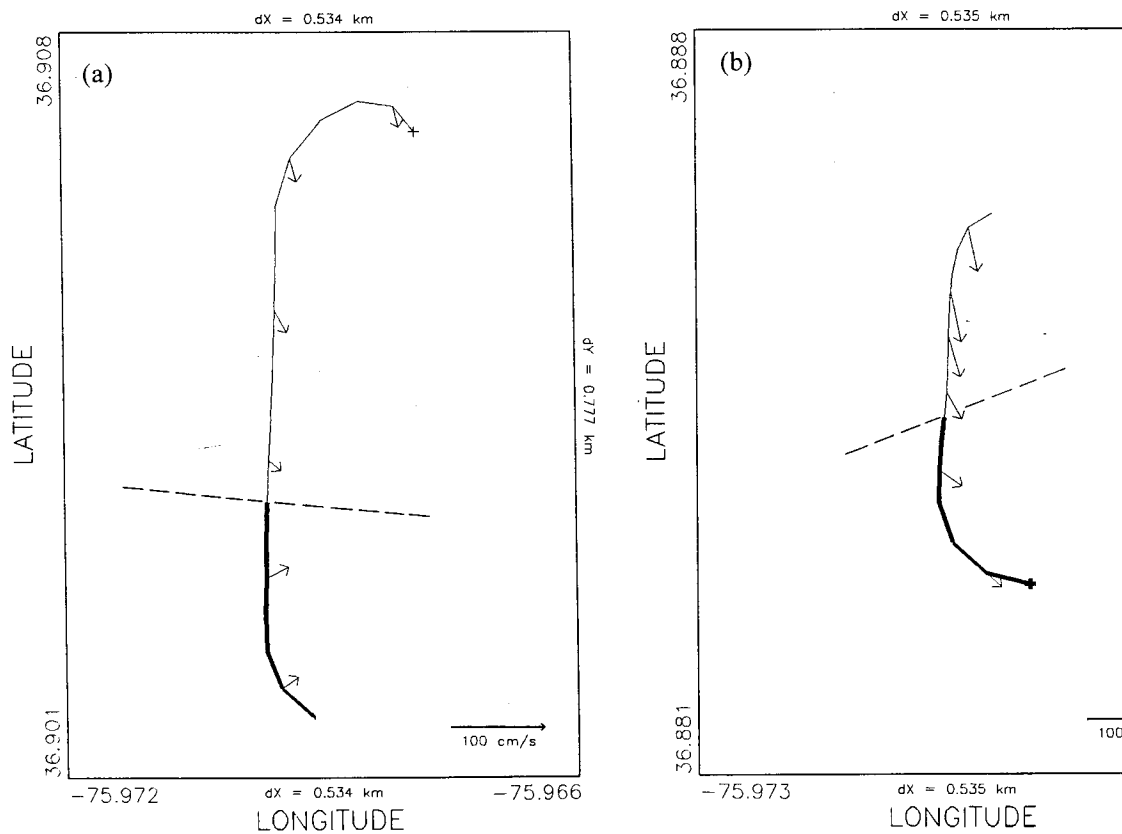


Fig. 8. Near-surface currents for 25 September 1996 frontal crossings shown in the previous figure at points 1 and 2, otherwise as in Fig. 4(a). (a) Crossing 4 (0849–0855 LT); (b) Crossing 14 (1015–1025 LT). Dashed lines show the approximate local frontal orientations at the time the ship crossed each.

made at + 5.5 h vs. + 5.4 h for the May 9 case, so it is interesting that these frontal positions are nearly coincident.

Some results from crossings 4 and 14 are shown in Fig. 8. Hydrographic conditions were very similar to the case on 9 May 1997. For both crossings 4 and 14, the water north of the front had a salinity of 22.5; ambient water south of the front had a salinity of 28.5 psu. A strong contrast in optical transmissivity was also found (not shown), the plume water having a value about a 10% lower than the ambient water. For crossing 4 (Fig. 8(a)) the near-surface flow on the plume-side of the front was about 30 cm/s and directed approximately southeastward. In the ambient water south of the front, the near-surface flow is about 20 cm/s and directed northeastward. The front was oriented approximately east–west (dashed line in the figure) so that the across-front convergence velocity was about 30 cm/s. Prior to crossing 4 (< 4 h into flood) visual observations and shipboard radar images showed a frontal apex similar to that found on 9 May (Fig. 3(c); 3.4 h into flood). The major changes observed at crossing 14 are an increase in southward flow in the plume water (because of a weakening flood) and southeast flow in the ambient water (because of tidally induced clockwise rotation of the current over time). The local front orientation also rotated toward the northeast so that the across-front convergence was still about 30 cm/s.

Fig. 9 shows for crossing 4 a vertical section of the acoustic backscatter intensity. This single example is representative of the other 14 crossings made. Ambient values of intensity are in the range of -92 to -104 dB. A core region of high intensity values ($I_{\max} \approx -72$ dB) descends steeply from near the surface and extends beneath the front.

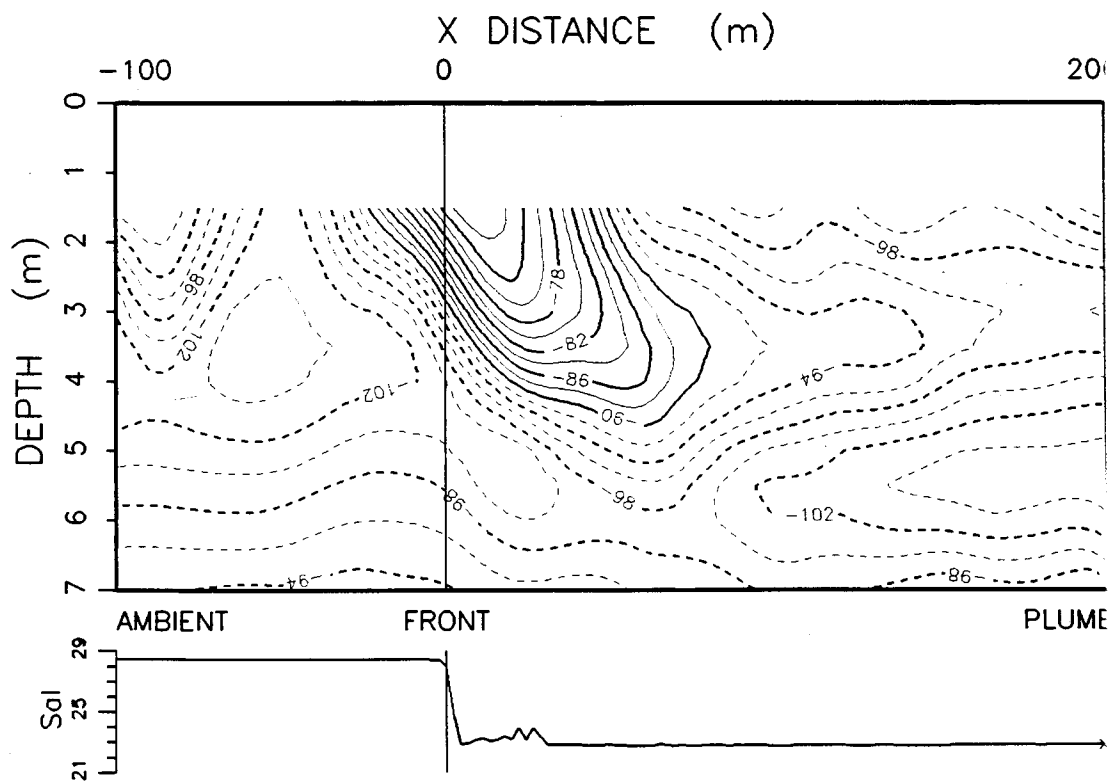


Fig. 9. Vertical section of acoustic backscatter intensity ($I \geq -90$ dB, solid contours) for frontal crossing 4 made on 25 September 1996, otherwise as in Fig. 4(b). Water depth is about 7.5 m.

the plume water. Values of $I \geq -90$ dB extend to a depth of about 4.5 m, which is quite similar to the 9 May example (Fig. 4(b)). This is strong evidence of subducting a bubble-enriched mixture of near-surface plume and ambient water. Unlike the 9 May case, the salinity decreases from its ambient to plume water value over a few meters and then shows a slight increase at about 20 m from the front on the plume side. (The salinity trace is shown at the bottom of Fig. 9.) This feature can be related to a frontal rotor as discussed by Luketina and Imberger (1987). Like the pattern of intensity contours suggests a frontally induced mixing layer into the underlying, denser fluid is entrained and mixed with the buoyant fluid. Note the occurrence of a relative maximum in intensity (the -86 to -90 dB contours) at depths of 4 to 3 m at 50 to 150 m from the front. A detailed comparison of the frontal circulation to the rotor-type model will be described in a subsequent paper.

The final example of in situ data is from 23 September 1996. Sampling in this case was conducted about 3 km north of Rudee Inlet during a period of strong (10-15 m/s) westerly winds. The ship made 17 transects approximately normal to shore over a 7.5 h period (0940–1710 LT), spanning early ebb to flood tide. Fig. 10 shows data from the second transect, made about 1 h before maximum ebb tide. Because of the strong ebb tidal current, the alongshore flow $v < 0$ across the entire section. (The positive alongshore flow direction (y -axis) is taken as 348° T.) A frontal feature is located about 3 km offshore and is oriented approximately alongshore. This is similar to the frontal feature shown in Fig. 2(d) except that it was sampled during flood tide. Seaward of the front is the outflow plume, which has strong southeastward flow, a salinity

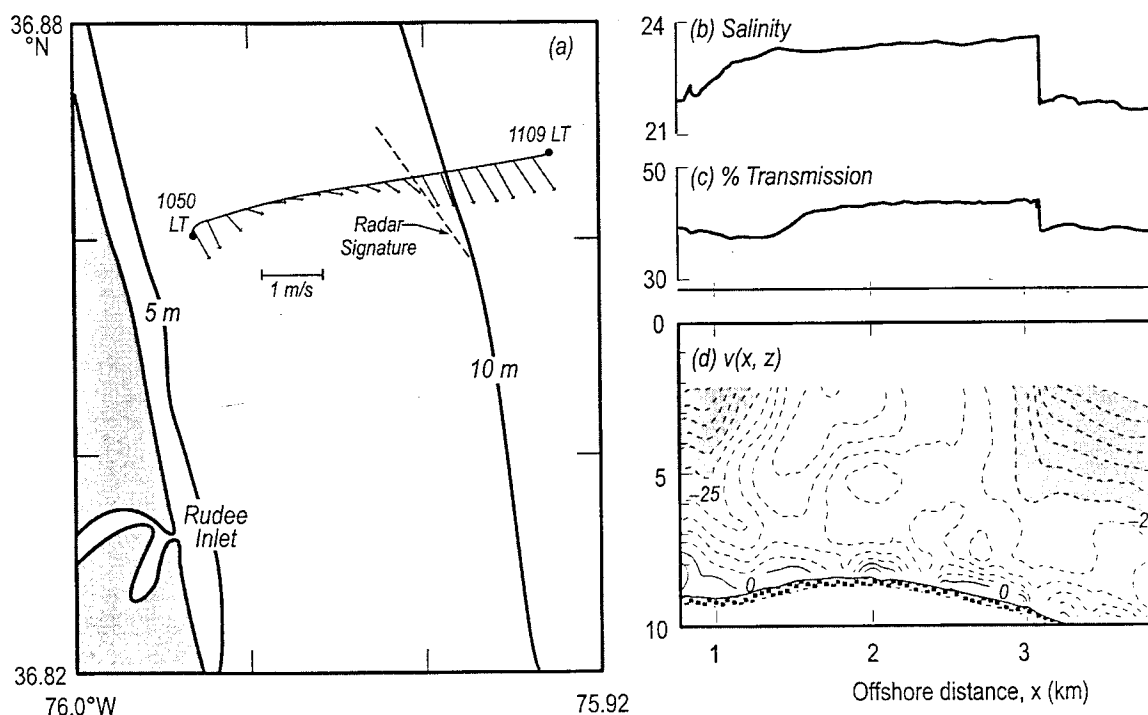


Fig. 10. Representative transect made north of Rudee Inlet on 23 September 1996 (1050 to 1109 LT). Vectors show 2 m depth current. Dashed line shows frontal orientation determined from shipboard imagery at the time the front was crossed, (b, c) near-surface salinity and optical transmissivity, (d) section of alongshore velocity v (positive toward 348° T); shading shows $v < -25$ cm/s.

about 22 psu, and relatively low values of optical transmissivity. As in the previous examples, the near-surface flow shows both across-front convergence and shear. Shoreward of the front is a 1.5 km wide band of generally weak flow ($v \approx -15$ cm/s) and higher salinity, which represents the dense water in this case. However, close inshore the salinity is again about 22, the optical transmissivity relatively low, and the flow strongly southward. Thus it appears the plume outflow has bifurcated farth upstream so that the band of dense water is sandwiched between and separates two streams of plume water. These separated streams are indicated in Fig. 6(d) by shaded regions denoting values $-50 \text{ cm/s} < v < -25 \text{ cm/s}$.

A combined analysis of all 17 transects (not shown) indicates that the salinity and relative velocity structure seen in Fig. 6 persists. In particular, there is a central region of relatively salty water that is flowing at about 40 cm/s northward relative to the plume water. Also, because the dense water does not extend continuously to the shoreline, it is unlikely to derive from a local upwelling response to the westerly (offshore) winds; thus the 23 September results may not be untypical ones. For example, a similar juxtaposition of water masses is suggested by the apparent northward intrusion of dense water seen in some of the radar images collected in May 1995 (e.g., Fig. 2(c)) and which occur near onset to flood and several kilometers from the coast. This final example thus serves to show that dense water may be found near the coast during ebb, setting the stage for frontogenesis near Cape Henry on the subsequent flood.

4. Discussion

4.1. Inshore vs. offshore fronts

A previous report of an estuarine outflow having both inshore and offshore fronts is given by Sanders and Garvine (1996), who collected in situ data across the Delaware Bay plume. As in our examples, their measurements were made during relatively high freshwater discharge. They found that the plume was concentrated over a 4–6 km wide region near the southern part of the bay mouth near Cape Henlopen, Delaware and that it was bounded by an offshore front, which extended seaward from within the bay mouth, and an inshore front, which overlaid a shoal crest extending seaward from Cape Henlopen. Both fronts were tidally modulated, with maximum horizontal density gradients occurring during early flood current. This is explained by Sanders and Garvine by the occurrence of the lowest salinity water in the near field during slack water before flood and by subsequent frontogenesis induced by convergence of the flooding tidal current in the area of the bay mouth.

In our observations, most cases show a distinct frontal segment near Cape Henry during flood but unlike the Delaware Bay there is no comparable shoal crest to orient the front. Instead, the section of the front oriented approximately across shore varies in position and can translate both to the north and south during parts of the tidal cycle (Table 1), and the section oriented along shore appears to meander over time (see Section 4.3 below). Similar to Sanders and Garvine's scenario, frontogenesis is favor-

near the mouth of the bay at Cape Henry because of the large horizontal difference between the plume and ambient water and because of surface convergence, which arises between the buoyant outflow and the ambient off Virginia Beach. The buoyant outflow can extend and dominate into 1 (Table 1). This is consistent with HF Doppler radar measurements made by COPE-1 by Haus et al. (1998) who report southward surface flow near Cape Henry extending into flood tide. The ambient current, which opposes and tends to cancel the outflow near Cape Henry, consists of the flooding tidal current possibly superimposed by a northward alongshore flow induced by an offshore anticyclonic eddy (see Section 4.2 below).

4.2. Flow recirculation as a source of dense coastal water

We observe dense water occurring along the coast under a variety of wind conditions as well as a tendency for northward (or relative northward) flow. Measurements made by Holderied and Valle-Levinson (2000), also made under conditions of relatively high discharge from the bay, also show evidence of dense water inshore near Cape Henry and northward flow along the coast. A possible source of northward flow along the Virginia coast north of Rudee Inlet is a mean anticyclonic eddy centered southeast of Cape Henry identified by Harrison et al. (1998). Might the dense water be related to such a circulation pattern? Under non-uniformly favorable winds, the coastal band would be fed by recirculating plume water that becomes saltier through entrainment of underlying shelf water or through mixing with residual, previously upwelled water along the coast. This is consistent with salinity values of 23 to 25 being found for westerly and northwesterly winds compared with plume salinities of about 22. Entrainment of relatively clear water would also account for the higher values of optical transmissivity found in the coastal band. During upwelling-favorable winds, the plume is displaced offshore by Ekman drift and higher-salinity water occurs near the coast (Ruzecki, 1988; Boicourt et al., 1987, Fig. 2). This higher salinity water can then directly feed the coastal band. This is consistent with a salinity of about 28 psu found for westerly winds (Table 1).

Two distinct mechanisms could create a mean anticyclonic eddy southeast of Cape Henry. One is separation of the outflow from the coast near Cape Henry. For example, model simulations done by Valle-Levinson et al. (1996; Fig. 9) and by Harrison et al. (1998; Fig. 2), both using a right-angle inlet-seashore geometry and steady winds, appear to show flow separation and a resulting advection of higher salinity water back toward the inlet mouth. However, our radar measurements show frontal features extending (nearly perpendicularly) toward shore, which suggests that the outflow from the bay hugs the coastline and hence does not separate at Cape Henry. Another mechanism is a residual tidal eddy (e.g., Chao, 1990). In this case, our measurements are too limited to draw any conclusion, but if such an eddy were present, its strength would wax and wane over the spring-neap tidal cycle. Some evidence for such a fortnightly modulation of an anticyclonic flow pattern appears in our radar measurements (see Fig. 7 in Marmorino et al., 1999c). However, this is

reflect modulation of the intensity of vertical mixing (proportional to the third power of the tidal current) and hence the stratification of the discharge water, which may have its own consequences for the inner-shelf hydrography (Simpson, 1997; Worster, 1998).

4.3. *Similarity to a tidal intrusion front*

In several respects, the front near Cape Henry is similar to an estuarine tidal intrusion front, which forms during flood tide as an inflow of dense seawater plunging (subducts) beneath ambient estuarine water (Largier, 1992). For the tidal intrusion front, when the intruding seawater is confined laterally by the sides of the estuary, lateral gradients in the flow result so that the front is not oriented perpendicular to the flow. The front is thus effective in diverting some of the inflow toward mid-stream so that the mid-stream velocity will increase toward the midstream plunge point, which in turn, is pushed farther downstream and into the less-dense water. The tidal intrusion front under these conditions exhibits a V-shaped plunge line. By analogy, we can consider the northward-flowing band of denser seawater to be confined by the Virginia shore to the west and by the plume to the east. East–west flow gradients may then likewise develop, leading to diversion of some of the inflow and formation of a V-shaped frontal apex. Evidence supporting this argument is the formation of a single, prominent frontal apex near Cape Henry under increasing flow amplitude during flood.

Bathymetry has been shown to play an additional role for the tidal intrusion front. Kuo et al. (1990a) shows how a tidal intrusion front (specifically, the front in the estuary of the James River, Virginia) may be stabilized in its position by an abrupt deepening of bathymetry, resulting in a quasi-steady hydraulic balance and a strong front. To investigate the possibility of this effect occurring in our dataset, all the radar images showing a clear V-shaped planform were analyzed and the positions of the frontal apex (the pointed tip of the “V”) were plotted on a bathymetric chart (Fig. 1). These tip positions vary spatially over several kilometers but consistently fall between the 8- and 10-m isobaths, and that depth range delineates the fall-off from the broad inshore region of 5 to 8 m depths toward the deep channel located north and east of Cape Henry (see Fig. 1). This result provides some evidence that the Kuo et al. mechanism may be at work. A similar bathymetric effect acting on the alongshore frontal segment is less clear as a detailed examination of the imagery from 9 May shows it to meander in position but to lie approximately along the 8 m isobath on average (Sletten et al., 1999). It is interesting to note that the alongshore segment of the tidal intrusion front in the James River estuary is also stabilized near the 8 m isobath.

Given the tendency of the front to recur near Cape Henry, what might be the fate of the subducted seawater? One possibility is that it cascades down the sloping bottom and then advects into the bay at a depth determined by its density relative to shelf water flowing in directly from offshore. The inflow of shelf water is observed to persist over the tidal cycle in that location (Holderied and Valle-Levinson, 2000). The

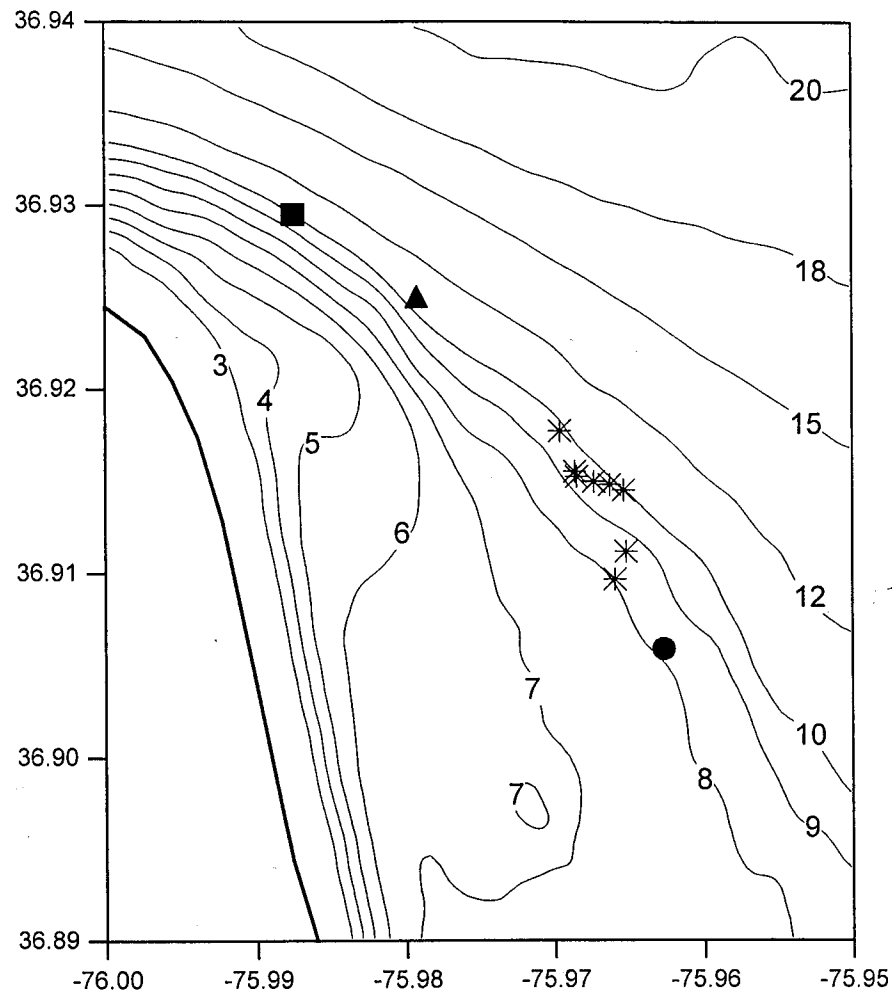


Fig. 11. Locations of the frontal apex for all observed cases of V-shaped planforms. Sources: 5 LT (Pass 10); 9 May, 1020–1215 LT (Passes 30–57; selected results shown); 16 May, 1344 LT (1 September, 0830 LT (ship's crossing 2).

circulation path, augmented perhaps by a residual eddy (Section 4.2), may a means to retain planktonic larvae near the mouth of the bay (e.g., Johnson to redistribute surface pollutants within the estuary. This again is similar to intrusion front, where frontal subduction allows surface particles (such larvae in the case of the James River estuary) to recirculate upstream against seaward estuarine circulation in the near-surface layer (Kuo et al., 1990b).

5. Summary and conclusions

We have described a recurring, nearshore front located over the inner continental shelf near Cape Henry, Virginia. The front occurs on the right-hand side seaward, of the buoyant plume discharging from the Chesapeake Bay and the plume water from an inshore band of relatively dense water. The front appears to be of a type similar to the inshore plume front reported by Sar Garvine (1996) for the Delaware Bay. The dense inshore water penetrates n

during flood tide to near Cape Henry, where it subducts beneath the buoyant outflow (as inferred from across-front sections of acoustic backscatter intensity) and evolves to a prominent V-shaped planform (as determined using microwave radar imagery). We have speculated that a residual eddy, possibly tidal in origin, contributes to the presence of dense water along the coast and to northward flow.

Very similar frontal behavior was found in data collected during two field campaigns despite a large difference in freshwater discharge rates. This suggests a “Cape Henry front” can be expected to occur under conditions of moderate to high discharge rates. The front appears to have several similarities to a classic tidal intrusion from a distinct frontal apex occurring during flood tide; horizontal constraints (coastline and plume); frontal subduction; and possible stabilization by a bathymetric gradient. These characteristics augmented perhaps by residual anticyclonic circulation may have consequences for the recirculation of near-surface material near the mouth of the bay.

Future field work might attempt to measure the genesis and ultimate demise of the frontal structure, aspects not captured in the present study. Also, a longer-term study could assess how the evolution of the inshore front may depend upon the spring-neap tidal cycle, reduced freshwater discharge, and other factors.

Acknowledgements

This paper is a contribution to the Physics of Coastal Remote Sensing Accelerated Research Initiative, which is funded by the Office of Naval Research and managed by the Naval Research Laboratory by Dr. Richard Mied. We thank Dr. Robert Arno for drawing our attention while at sea to the interesting fronts found near Cape Henry, the master and crew of the R/V *Cape Henlopen* and the Naval Research Laboratory Flight Support Detachment for their cooperation and help in support of the field work, and Dr. Dennis Trizna for access to the imagery from the shipboard radar system. Comments from several colleagues, including Dr. Don Johnson and Dr. Arnaldo Valle-Levinson, and two anonymous reviewers were helpful in preparing the final manuscript.

References

- Boicourt, W.C., Chao, S.-Y., Ducklow, H.W., Glibert, P.M., Malone, T.C., Roman, M., Sanford, J., Fuhrman, J., Garside, C., Garvine, R., 1987. Physics and microbial ecology of a buoyant estuarine plume on the continental shelf. *Eos* 69, 666–668.
- Chao, S.-Y., 1988. Wind-driven motion of estuarine plumes. *Journal of Physical Oceanography* 18, 1144–1166.
- Chao, S.-Y., 1990. Tidal modulation of estuarine plumes. *Journal of Physical Oceanography* 20, 1115–1135.
- Chao, S.-Y., 1998. Hypopycnal and buoyant plumes from a sediment-laden river. *Journal of Geophysical Research* 103, 3067–3081.
- Harrison, W., Brehmer, M.L., Stone, R.B., 1964. Nearshore tidal and non-tidal currents, Virginia Beach, Virginia. U.S. Army Coastal Engineering Research Center, Tech. Memo. No. 5, 20 pp.

- Haus, B.K., Graber, H.C., Shay, L.K., 1998. Tidal modulation of surface flows in the turning the Chesapeake Bay outflow. *Eosmaw Transactions AGU*, 79(1). Ocean Sciences Meeting OS158.
- Holderied, K., Valle-Levinson, A., 2000. Hydrographic and flow structure in the Chesapeake and plume region under high freshwater discharge conditions. *Continental Shelf Research*.
- Johnson, D.R., 1995. Wind forced surface currents at the entrance to Chesapeake Bay: their effect on crab larval dispersion and post-larval recruitment. *Bulletin of Marine Science* 57, 726–738.
- Kuo, A.Y., Byrne, R.J., Hyer, P.V., Ruzecki, E.P., Brubaker, J.M., 1990a. Practical application of tidal-intrusion fronts. *Journal of Waterway, Port, Coastal, and Ocean Engineering* 116, 34.
- Kuo, A.Y., Ruzecki, E.P., Neilson, B.J., Brubaker, J.M., Byrne, R.J., 1990b. Circulation and transport of oyster larvae in Virginia estuaries.
- Largier, J.L., 1992. Tidal intrusion fronts. *Estuaries* 15, 16–39.
- Luketina, D.A., Imberger, J., 1987. Characteristics of a surface buoyant jet. *Journal of Coastal Research* 92, 5435–5447.
- Marmorino, G.O., Trump, C.L., 1996. High-resolution measurements made across a tidal intrusion. *Journal of Geophysical Research* 101, 25 661–25 674.
- Marmorino, G.O., Trump, C.L., Hallock, Z.R., 1999a. Near-surface current measurements using a deployed “horizontal” ADCP. *Journal of Atmospheric and Oceanic Technology* 10, 1456–1466.
- Marmorino, G.O., Trump, C.L., Trizna, D.B., 1999b. Preliminary observation of a tidal intrusion inside the mouth of the Chesapeake Bay. *Estuaries* 22, 105–112.
- Marmorino, G.O., Shay, L.K., Haus, B.K., Handler, R.A., Graber, H.C., Horne, M.P., 1999. Analysis of HF Doppler radar current measurements of the Chesapeake Bay buoyant outflow. *Continental Shelf Research* 19, 271–288.
- Miller, J., 1998. Airborne salinity mapper makes debut in coastal zone. *Eosmaw, Transactions Geophysical Union* 79, 173–177.
- O'Donnell, J., Marmorino, G.O., Trump, C.L., 1998. Convergence and downwelling at a river plume. *Journal of Physical Oceanography* 28, 1481–1495.
- Ruzecki, E., 1981. In: Campbell, J.W., Thomas, J.P. (Eds.), *Temporal and spatial variability of the Chesapeake Bay plume*. NASA Conference Publication 2188, Chesapeake Bay Plume Study, 1980.
- Sanders, T.M., Garvine, R.W., 1996. Frontal observations of the Delaware Coastal Current south of Chesapeake Bay. *Continental Shelf Research* 16, 1009–1021.
- Sletten, M.A., Marmorino, G.O., Donato, T.F., McLaughlin, D.J., Twarog, E., 1999. An aircraft-based aperture radar study of the Chesapeake Bay Outflow Plume. *Journal of Geophysical Research* 104, 1211–1222.
- Simpson, J.H., 1997. Physical processes in the ROFI regime. *Journal of Marine Systems* 12, 3–13.
- Thorpe, S.A., 1982. On the clouds of bubbles formed by breaking wind-waves in deep water, and on the air-sea gas transfer. *Philosophical Transactions of Royal Society of London A* 304, 155–199.
- Valle-Levinson, A., Klinck, J.M., Wheless, G.H., 1996. Inflows/outflows at the transition between the estuary and the coastal ocean. *Continental Shelf Research* 16, 1819–1847.
- Volgelzang, J., Ruddick, K.G., Moens, J.B., 1997. On the signatures of river outflow fronts in radar images. *International Journal of Remote Sensing* 18, 3479–3505.
- Wiseman, W.J., Garvine, R.W., 1995. Plumes and coastal currents near large river mouths. *Estuaries* 18, 509–517.
- Wong, K.-C., 1998. On the variability in the vertical structure of the Delaware coastal current. *Continental Shelf Research* 18, 929–940.